

Time measurement of scintillator detector based on Belle II KLM upgrade

Xiyang Wang^a, Shiming Zou^a, Xiaolong Wang^{a,*}, Yugang Ma^{a,b,**}, Deqing Fang^{a,b}, Ziyu Liu^c, Hongyu Zhang^a

^aKey Laboratory of Nuclear Physics and Ion-beam Application (MOE) and Institute of Modern Physics, Fudan University, 220 Handan Road, Shanghai, 200433, China

^bShanghai Research Center for Theoretical Nuclear Physics, NSFC and Fudan University, Shanghai, 200438, China

^cSchool of Physics, Nankai University, 94 Weijin Road, Nankai District, Tianjin, 300071, China

Abstract

The upgrade proposal for the Belle II experiment focuses on improving the time resolution for the KLM detector. We investigated the feasibility of incorporating Time-of-Flight system for muon and K_L detections within the Belle II KLM framework, which utilizes plastic scintillators and SiPM readouts. To achieve this, we developed high speed front-end electronics and arrays optimized for SiPM detection. By implementing constant fraction timing and employing a weighted average of dual-end timing, we significantly enhanced the timing accuracy for particle detection. Comprehensive testing and analysis show that a plastic scintillator measuring 135 cm in length is capable of achieving a time resolution of (70 ± 7) ps. Furthermore, a shorter 50 cm plastic scintillator can achieve a time resolution of (47 ± 2) ps.

Keywords: Time-of-Flight, time resolution, Muon detector, scintillator, SiPM

1. Introduction

In particle and nuclear physics experiments, determining the four-momentum of neutral hadrons, such as the K_L mesons and neutrons, presents significant challenges. High-energy frontier experiments like ATLAS [1] and CMS [2] employ costly hadron calorimeters (HCALs) that achieve energy resolutions of approximately 40% – 50%. In contrast, intensity frontier experiments such as BaBar [3], Belle [4], Belle II [5], and BESIII [6] do not utilize HCALs for measuring the energy of neutral hadrons with momenta of 1 GeV/c – 5 GeV/c, primarily due to the limited energy resolution achievable by HCALs in this momentum region. However, the momentum of a neutral hadron can also be determined according to the time of its flight (T_{fly}).

As a super B-factory experiment, the Belle II experiment aims to explore new physics at the forefront of high luminosity while improving the precision of measurements for Standard Model parameters [7]. The K_L

and muon detector (KLM), located at the outermost layer of the Belle II detector, is the largest subdetector [8]. We described in the Conceptual Design Report (CDR) of the Belle II upgrade that the KLM system can be upgraded to have the new capability of Time-of-Flight (TOF) measurement [5] for directly determining the momentum of a long-lived neutral hadron particle, such as K_L or neutron. For this purpose, new TOF technology needs to be developed. On the other hand, since the volume of KLM is huge, the cost of such new technology must be low.

Traditional TOF detectors predominantly use two technological approaches. The first approach employs multi-gap resistive plate chambers (MRPCs), as seen in detectors such as the STAR [9], ALICE [10], and BESIII endcap TOF [11]. MRPCs can generally achieve a high time resolution of 50 – 60 ps. However, notable drawbacks include their complex structures, which require gas flow systems, and their susceptibility to gas contamination (e.g., $\text{C}_2\text{H}_2\text{F}_4/\text{C}_4\text{H}_{10}/\text{SF}_6$), and the number of readout channels. The second and more traditional approach utilizes plastic scintillators coupled with photomultiplier tubes (PMTs), such as Belle TOF [12] and BESIII barrel TOF [13]. Due to the inherent transit time spread of PMTs, achieving very high time resolution is challenging.

*Corresponding author.

Email: xiaolong@fudan.edu.cn

**Corresponding author.

Email: mayugang@fudan.edu.cn

Corresponding author.

Email: dqfang@fudan.edu.cn

Silicon photomultipliers (SiPMs) represent a promising alternative, offering high time resolution and insensitivity to magnetic fields. Currently, some experiments have successfully employed SiPMs in conjunction with small-sized scintillators (length ≤ 15 cm) to construct TOF detectors, achieving time resolutions better than 100 ps, as demonstrated by the PANDA [14] and AMS-100 [15] experiments. However, only a few applications use SiPMs with large, elongated scintillators. The principal challenges for these applications include the scintillator's attenuation length, high noise levels in SiPM arrays, and issues related to slow rise times.

This paper presents an innovative scintillation detection approach that enhances the foundational scheme employed in the KLM system. Since 2018, our laboratory at Fudan University has been working with the GaoNengKeDi Company in Beijing to develop new scintillators for high time resolution and low cost. We significantly improve the time resolution achievable with scintillators by utilizing scintillation materials with extended attenuation lengths and a detection array comprising large SiPMs and ultrafast front-end electronic readouts.

2. Belle II KLM and the upgrade

As the outermost component of the Belle II detector, the KLM identifies K_L mesons and muons with momenta of up to 4.5 GeV/c. As illustrated in Fig. 1(a), the KLM extends from radii of 200 cm to 240 cm in the octagonal barrel and from 130 cm to 340 cm in the forward and backward endcaps. The barrel section consists of 15 detector layers interspersed with 14 layers of yoke iron, while each endcap contains 14 detector layers and 14 layers of iron. The yoke acts as a magnetic flux return for the solenoid and aids in hadronic cascade clustering for K_L detection.

The large-surface-area detector panels are approximately 3.1 cm thick and are positioned between 4.7 cm steel plates. In these panels, the innermost two layers of the barrel and all layers of the endcaps are equipped with extruded scintillator strips, while the remaining 13 layers of the barrel utilize legacy RPCs from the Belle experiment. Each detector panel provides two orthogonal position measurements for a through-going particle via hits on the scintillator strips. The KLM features around 38,000 readout channels, with approximately half allocated for scintillator detection.

In the scintillator modules, the cross section of each barrel scintillator strip measures 4 cm \times 1 cm, while the endcap strip measures 4 cm \times 0.75 cm. Each scintillator strip contains a Kuraray Y11(200)MSJ wavelength-

shifting (WLS) fiber [16], which collects emitted photons from the extruded scintillator and directs them to a SiPM, also known as a Multi-Pixel Photon Counter (MPPC: Hamamatsu S10362-13-050C). The MPPC is directly coupled to one end of the WLS fiber. Signals are preamplified internally by a factor of approximately 10 before being routed via ribbon cables to external readout electronics mounted on the magnet yoke. We tested the time resolution of the preamplifier to be about 0.5 ns.

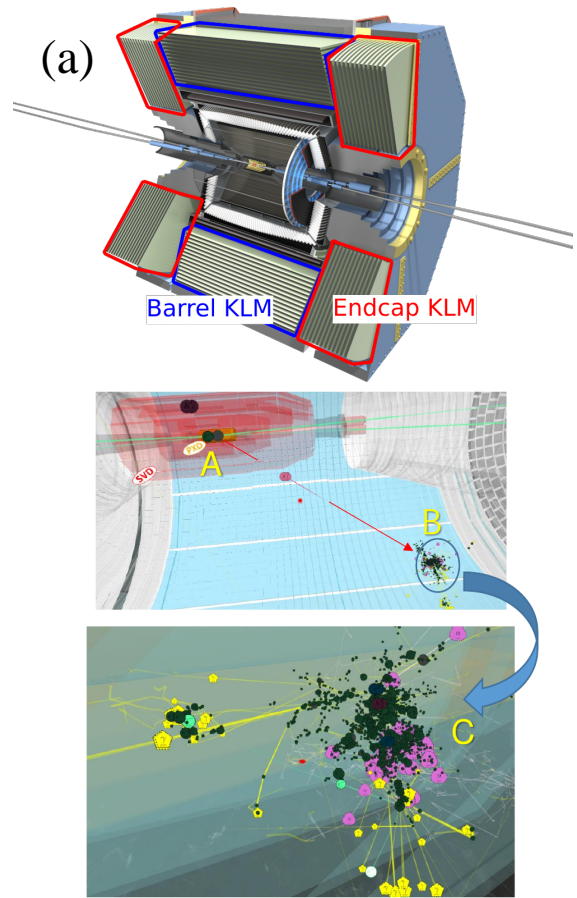


Figure 1: (a) The KLM system in the Belle II detector and (b) a hadronic cluster generated by a K_L meson in the Belle II virtual reality.

In the CDR of the Belle II upgrade [5], we described the idea for adding the capability of **energy measurement for K_L meson via a time-of-flight measurement in new scintillator bars**. Figure 1(b) illustrates a hadronic cluster generated by a K_L meson, as depicted in the Belle II virtual reality simulation [17]. The simulation data indicate multiple hits within this hadronic cluster. Our analysis suggests that measuring the time

of flight of the K_L meson is feasible based on the rapid hits [18].

Accurate determination of the T_{fly} for a K_L meson requires precise measurements of the start time (T_{start}) and stop time (T_{stop}). The T_{start} is derived from the collision time at the SuperKEKB accelerator, which has a resolution better than 32 ps [19]. Considering the typical lifetime of a B meson or D meson produced at the interaction point (IP) is approximately 10 ps, the expected resolution for T_{start} is anticipated to be better than 35 ps. Meanwhile, the T_{stop} is determined from the timing information of multiple hits within a hadronic cluster detected by the upgraded KLM system [8]. Assuming a time resolution of 100 ps for T_{stop} and a typical flight distance of 200 cm from the IP to the new KLM in Belle II, the momentum resolution for a K_L meson with a momentum of 1.5 GeV/ c can achieve a value of 0.19 GeV/ c , corresponding to a relative uncertainty of 13%. This enhanced ability to measure four-momentum improves the momentum resolution of the parent particle in decay modes involving a K_L meson in the final state, such as $B^0 \rightarrow J/\psi K_L$, while also reducing accidental backgrounds in these decay processes. However, the existing scintillation detection scheme in the KLM currently achieves only 1 – 2 ns time resolution according to the test in our laboratory [20], which is insufficient for optimal performance, highlighting the necessity for an upgraded detection scheme.

3. Improvements to the scintillation detector design

As we described for the new KLM detection scheme in the Belle II Upgrade CDR [5], several key improvements have been implemented to achieve a high time resolution.

- Removal of WLS fibers: The WLS fibers in the scintillator were removed, and instead, a thicker scintillator with higher light yield and longer attenuation length was employed
- Design of SiPM array with high-speed amplifier: arrays of large size SiPMs are used for photon collection. The τ_{rise} of the SiPM array has been further reduced by employing a hybrid connection. Meanwhile, high-bandwidth, low-noise SiPM front-end preamplifiers have been employed to enhance the quality of the SiPM output signal.
- Double-ended readout scheme: inspired by time-of-flight (TOF) detector readout techniques, we have transitioned from a single-ended to a double-ended readout scheme to significantly improve the

time resolution at positions far from the SiPM readout end.

For this study, we sourced plastic scintillators from two manufacturers: Saint-Gobain Company [21] and GaoNengKeDi Company [22]. The BC420 scintillator from Saint-Gobain, known for its benchmark quality in TOF measurements, serves as a reference for evaluating cost-effective alternatives from GaoNengKeDi. The dimensions of the BC420 scintillator are 5 cm \times 3 cm \times 120 cm, with a Bulk Light Attenuation Length (L_{Att}) of 110 cm [21]. In contrast, GaoNengKeDi has developed various elongated plastic scintillator strips that demonstrate superior light transmission capabilities, particularly in comparison to those produced using extrusion methods. Throughout our tests in the past years, GaoNengKeDi has significantly improved their scintillators' L_{Att} and light yields.

As illustrated in Fig. 2(a), we cataloged the GaoNengKeDi scintillators with dimensions ranging from 4 cm \times 2 cm \times 50 cm to 4 cm \times 2 cm \times 150 cm, categorized by the shipment date of the samples: GNKD_1, GNKD_2, GNKD_3, and GNKD_4. The BC420 scintillator is also depicted in Fig. 2(a).

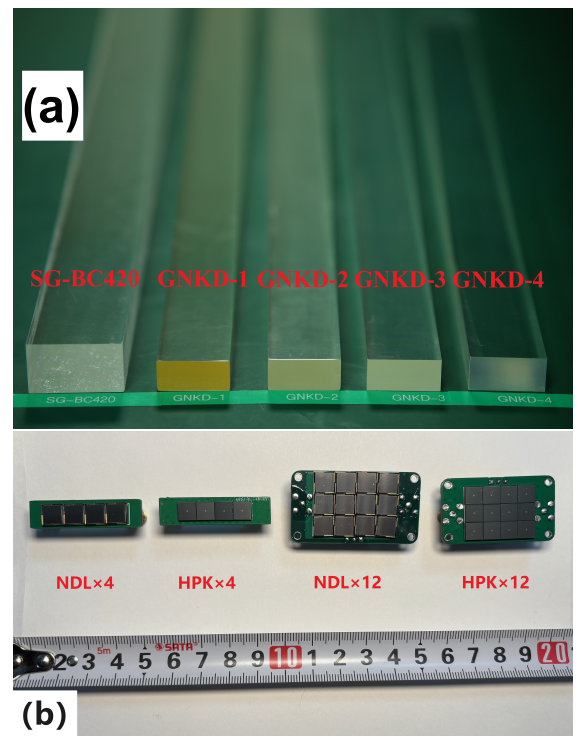


Figure 2: (a) BC420 scintillator sample from Saint-Gobain and different scintillator samples from GaoNengKeDi. (b) Various configurations of SiPM arrays, featuring a preamplifier located on the back of the PCB.

All the SiPMs used in this study measure 6 mm × 6 mm, including the S14160-6050 from Hamamatsu (HPK) [23] and the EQR20-11-6060 from Novel Device Laboratory (NDL) [24]. We further enhance the time resolution by configuring the SiPMs into series or parallel arrangements, thereby creating SiPM arrays [25], as illustrated in Fig. 2(b). Detailed findings from these tests are presented in Sec. 5.1.

To minimize noise and interference during signal transmission, both the front-end amplifier and the SiPM array are mounted on the same printed circuit board (PCB). The preamplifier is designed using the ultra-low noise, high-bandwidth operational amplifier LMH6629 from Texas Instruments [26]. Our preamplifier provides a gain of +26 dB and a bandwidth of 426 MHz, facilitating a τ_{rise} of 1 ns while reducing baseline noise to as low as 0.6 mV [27]. The performance of the preamplifier is crucial for achieving the exceptional time resolution characteristic of the SiPM array.

4. Cosmic ray measurement setup

We utilize cosmic rays to evaluate the performance of the scintillator, as illustrated in Fig. 3. The trigger system consists of two 10 cm strips positioned at the top and bottom of the scintillator to identify the impact location and hit time of cosmic rays. Dual-end readouts are employed to collect photon data from both ends of the strip, thereby enhancing overall time resolution. This dual-end readout strategy is also applied to the triggers to mitigate the “time walk” effect caused by positional uncertainty in cosmic ray impacts. Notably, the trigger location is strategically placed at the midpoint of the elongated strip, where time performance typically exhibits reduced accuracy.

For signal digitization, we employ a Tektronix MSO58 oscilloscope, which features a sampling rate of 6.25 GS/s and an analog bandwidth of 1 GHz, meeting the requirements for high-speed signal digitization. For multi-channel acquisition, we also utilize a desktop digitizer, the DT5742, as an alternative to the oscilloscope. This digitizer can handle 16 channels with a sampling rate of 5 GS/s and a bandwidth of 500 MHz, delivering excellent performance in high-speed signal acquisition applications [28].

Upon digitizing the waveform with an oscilloscope or digitizer, the resulting data is processed offline on a computer. In the case of elongated strip-shaped scintillation detectors, significant disparities in signal amplitude often exist between the far and near ends. Utilizing the leading edge timing method in such cases may lead

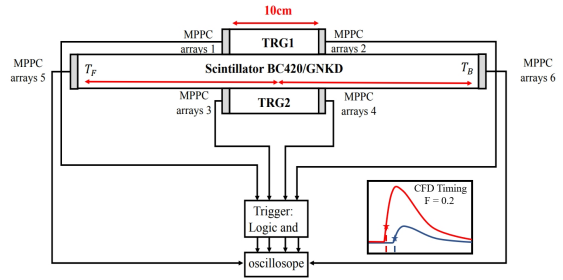


Figure 3: Experimental setup for cosmic ray testing of the scintillator. The readout system at each end of the trigger consists of four SiPMs, while the readout at each end of the scintillator being measured is composed of 12 SiPMs to accommodate its larger cross section area.

to considerable timing inaccuracies. To mitigate this issue, it is essential to fit the rising edge of the waveform and subsequently apply Constant Fraction Discrimination (CFD) timing. The resulting time spectrum is then fitted to determine the time resolution, as illustrated in Fig. 4. Additionally, the digital waveform provides valuable information regarding pulse amplitude.

Accurately determining the high precision trigger time T_0 is crucial for high time resolution tests. As shown in Fig. 3, the trigger time T_0 of the test system is calculated by averaging the times recorded by two short triggers: $T_0 = (T_1 + T_2 + T_3 + T_4)/4$. Here, from T_1 to T_4 are the recorded time from SiPM array#1 to array#4 of the trigger system, as shown in Fig. 3. The time difference between the two triggers, denoted as $\Delta T_{\text{trg}} = (T_1 + T_2)/2 - (T_3 + T_4)/2$, allows us to calculate the time resolution of T_0 , represented as $\sigma_{T_0} = \sigma_{\Delta T_{\text{trg}}}/2$.

By using a series connection of four S14140-6050 MPPCs for the trigger readout, the time resolution of the test system T_0 can achieve a precision of 50 ps. The discrepancy between the average times T_F and T_B and the trigger time T_0 is given by $\Delta T_{\text{SC}} = (T_F + T_B)/2 - T_0$. Here, T_F and T_B are the time recorded by the SiPM array#5 and array#6 for the high time resolution scintillation under test, as shown in Fig. 3. By subtracting the uncertainty of T_0 , we obtain the time resolution of the long scintillator via

$$\sigma(T_{\text{ToF}}) = \sqrt{\sigma(\Delta T_{\text{SC}})^2 - \sigma(T_0)^2}. \quad (1)$$

5. Test results and analysis

5.1. Testing of SiPM array quantity and connection methods

As illustrated in Fig. 3, our experimental setup utilized a trigger measuring 10 cm in length with a cross

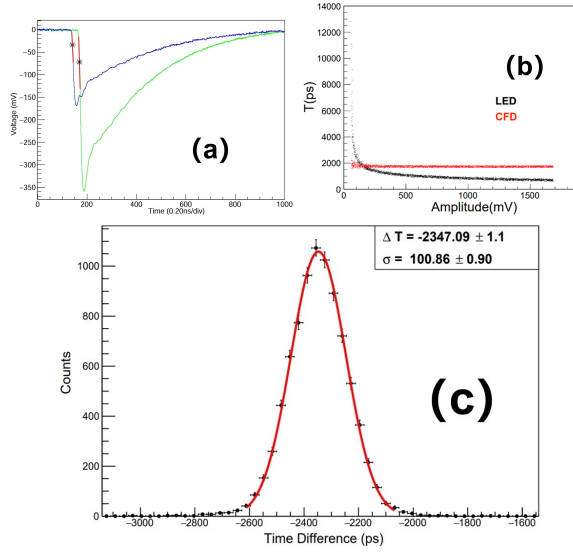


Figure 4: (a) Schematic representation of the timing method principle. (b) The relationship between timing and waveform amplitude after applying the CFD timing method. (c) The distribution of the time difference ΔT_{trg} alongside the best-fit result using a Gaussian function.

section of $4 \text{ cm} \times 1 \text{ cm}$. To facilitate effective photon detection for high time resolution, we employed an array consisting of four SiPMs. We investigated the time resolution using two connection configurations: parallel (4P) and series (4S), as shown in Fig. 5(a). The results indicate that the SiPM array connected in series exhibited superior time resolution compared to the parallel configuration. Specifically, the time resolution achieved with the Hamamatsu S14160-6050 surpassed that of the EQR20 SiPM from NDL. When operating at the optimal voltage, the 4S configuration yielded a time resolution of $\sigma(\Delta T_{\text{trg}}) = (104 \pm 4) \text{ ps}$, corresponding to a calculated time resolution of the trigger system of $\sigma(T_0) = (52 \pm 2) \text{ ps}$.

Since the scintillators being tested have large cross-sectional areas, i.e., $4 \text{ cm} \times 2 \text{ cm}$ of GaoNengKeDi samples and $5 \text{ cm} \times 3 \text{ cm}$ of BC420, an extensive array using 12 SiPMs is required to ensure efficient light collection. To address this, we tested the arrays in three distinct connection configurations: pure series (12S), pure parallel (12P), and a hybrid of series and parallel (4S3P). The results of these tests are presented in Fig. 5(b).

Connecting SiPMs in a pure parallel configuration increases the input junction capacitance of the amplifier, resulting in a slower τ_{rise} of the signal, large baseline noise, and increased timing uncertainty. In contrast, connecting SiPMs in a pure series configuration effectively mitigates these issues. This arrangement signifi-

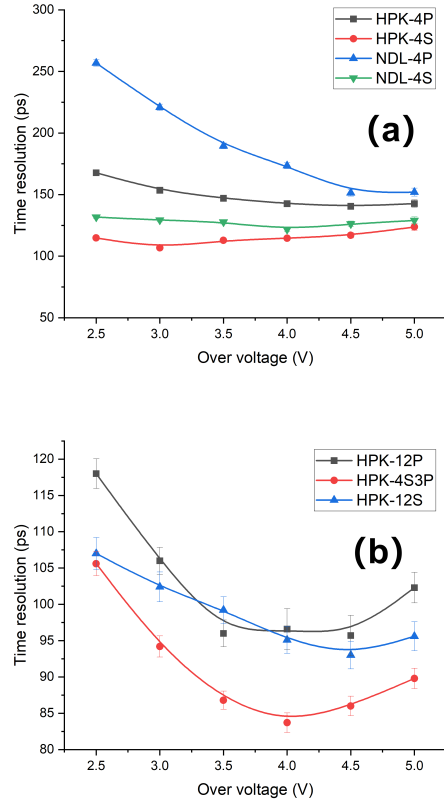


Figure 5: Comparison of connection modes for SiPM arrays and their effect on the time resolution as a function of overvoltage. Plot (a) displays the timing performance of triggers utilizing different SiPM read-out configurations, with the plastic scintillator sourced from GNKD. Plot (b) illustrates the timing resolution performance of the SG BC420 plastic scintillator.

cantly improves the τ_{rise} of the SiPM signal waveform from 12.4 ns in the 4P configuration to 4.1 ns in the 4S configuration, thereby enhancing time resolution. However, increasing the number of SiPMs in series does not lead to a significant improvement in τ_{rise} ; for instance, the τ_{rise} only marginally decreases from 4.1 ns in the 4S3P configuration to 4.0 ns in the 12S configuration. Additionally, a longer signal path for SiPM signals to reach the amplifier in larger configurations may degrade time resolution. Therefore, we choose the 4S3P hybrid configuration for the array of 12 SiPMs. In the test which will be described in Sec. 5.3, the hybrid configuration yields a time resolution of $\sigma(T_{\text{BC420}}) \approx 84 \text{ ps}$ at the midpoint of the 120 cm BC420 scintillator.

The operational voltage of the SiPM also has a substantial impact on time resolution. Our test results indicate that increasing the voltage enhances the photon de-

tection efficiency of the SiPMs, improves the signal-to-noise ratio (SNR), and subsequently boosts time resolution. However, excessively high overvoltage can significantly increase the dark count rate and crosstalk within the SiPM, diminishing the SNR and negatively affecting time resolution. Therefore, selecting the appropriate operating voltage is critical for optimal time resolution.

5.2. Single-end time resolution of various plastic scintillators

By adjusting the positions of the upper and lower short triggers, we can evaluate the average signal amplitude and time resolution at various locations along the scintillator. This methodology enables us to determine the scintillator's time resolution and attenuation length across different positions. Figure 6 illustrates the signal amplitude and time resolution at diverse hit positions.

The attenuation length L_{Att} of the scintillator is calculated through the exponential fitting of the average amplitude of the SiPM signals recorded at varying locations. It is crucial to emphasize that L_{Att} should reflect the intrinsic attenuation length of the scintillator while minimizing the influence of reflected light during the measurements. The effect of reflected light is more pronounced near the SiPM readout ends. Consequently, we selected data points situated more than 50 cm from the readout end for fitting. This approach yielded the following attenuation lengths for scintillators from different batches: $L_{Att} = (65 \pm 9)$ cm for GNKD_1, (70 ± 2) cm for GNKD_2, (120 ± 7) cm for GNKD_3, and (82 ± 8) cm for BC420. More information can be found in Table 1. Due to the short length of the GNKD_4 scintillator (50 cm), its decay length is not measured.

The time resolution of scintillators is strongly related to the number of photons collected by the SiPM arrays, as shown in Table 1. All scintillators achieve high photon collection efficiency of over 200 $p.e.$ and exhibit excellent time resolutions of approximately 60 ps at the near end. However, as the hit position moves farther away, the number of photons collected by the SiPM gradually decreases. Scintillators with longer L_{Att} and higher light yields, such as GNKD_3, can achieve better time resolution. Nevertheless, its time resolution declines from (53 ± 2) ps at the near end to (140 ± 6) ps at far end. Therefore, the implementation of a dual-end readout scheme is essential.

5.3. Time resolution test with dual-end readout

When employing a single-end readout, the time resolution progressively deteriorates as the hit position

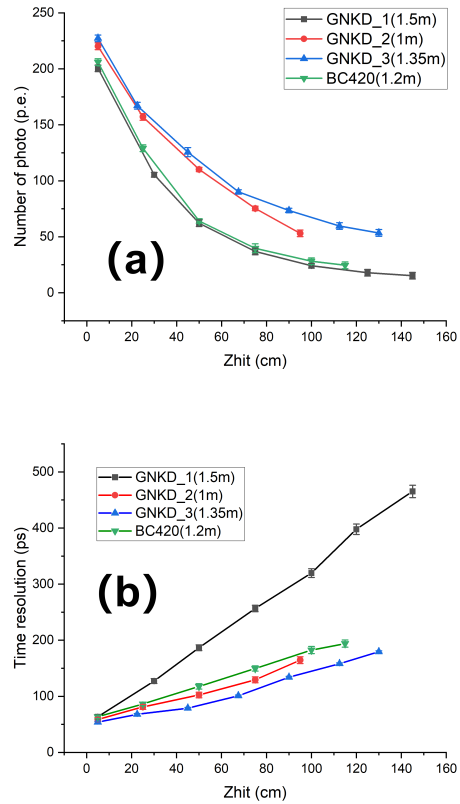


Figure 6: Variation of photon collection (a) and single-ended time resolution (b) as a function of cosmic ray hit position.

moves farther from the readout end. This issue can be effectively mitigated using a dual-end readout system that averages the time information from both ends. We adopt a strategy similar to that used in TOF detectors [29]. The resolution of T_{SC} is determined based on the weighted average of the times from both ends:

$$T_{SC} = \frac{T_F \sigma_F^{-2} + T_B \sigma_B^{-2}}{\sigma_F^{-2} + \sigma_B^{-2}}, \quad (2)$$

$$\sigma_{T_{SC}}^{-2} = \sigma_F^{-2} + \sigma_B^{-2}, \quad (3)$$

where X is the distance from the cosmic ray hit position to the readout end, $v \approx 14.7$ cm/ns is the speed of light propagation in the scintillator, $T_F = T_0 + X/v$, and $T_B = T_0 + (L - X)/v$.

Due to uncertainties in the hit position, the time T_{SC} is influenced by the position of the muon hit after weighted averaging. Although we utilize a short scintillator with a length of 10 cm as the trigger, this dimension still results in considerable uncertainty in determining the hit position. Notably, except at the midpoint of

Table 1: Comparison of photon collection and time resolution at the near-end and far-end of scintillators with different L_{Att} .

Type	$W \times H \times L$ (cm ³)	L_{Att} (cm)	Time Resolution (ps)		Collected Photons ($p.e.$)	
			$Z_{\text{hit}}=5$ cm	$Z_{\text{hit}}=95$ cm	$Z_{\text{hit}}=5$ cm	$Z_{\text{hit}}=95$ cm
SG-BC420	$5 \times 3 \times 120$	82 ± 8	63 ± 4	175 ± 6	206	30
GNKD_1	$4 \times 2 \times 150$	65 ± 3	63 ± 4	307 ± 8	200	26
GNKD_2	$4 \times 2 \times 100$	70 ± 9	59 ± 4	164 ± 6	220	53
GNKD_3	$4 \times 2 \times 135$	120 ± 7	53 ± 2	138 ± 6	227	70
GNKD_4	$4 \times 2 \times 50$	/	44 ± 3	$81 \pm 5(45 \text{ cm})$	341	154 (45 cm)

the scintillator, where the weighting factors from both ends are nearly equal, the time discrepancy caused by uncertainties in the impact position can be mitigated. One method to decrease the uncertainty of the hit position is by reducing the trigger length while increasing its height. However, this approach also leads to a substantial decrease in cosmic ray flux and an increase in measurement time. Each position was tested over two weeks to gather a sufficient statistical sample (more than 1,000 events). Consequently, we propose a multi-trigger testing scheme, as shown in Fig. 7(a). The trigger signals are shaped into different pulse widths ($\tau_1 = 50$ ns, $\tau_2 = 100$ ns, $\tau_3 = 150$ ns) and input to the TR0 interface of the DT5742. During data analysis, we can determine the location of cosmic ray hits using different pulse widths, allowing us to measure multiple positions simultaneously and significantly improve testing efficiency.

To effectively illustrate the improvement in time resolution at the far ends of the scintillator using dual-end readout, we conducted tests with the GNKD_3 scintillator. Figure 7(b) presents the results of the time resolution assessment with dual-end readout. We observed that the time resolution is least favorable at the center of the scintillator, measuring (70 ± 9) ps, while optimal resolution reaching about 50 ps is achieved at both ends. Notably, with dual-end readout, the position with the poorest time resolution typically occurs at the center, highlighting a key distinction from single-end readout methodologies. Additionally, we compared the time resolution obtained using Eq. (2) with that derived from the weighted average of T_F and T_B . This comparison demonstrated a strong correlation between the two sets of results.

Drawing from the insights obtained from the test results, we can extrapolate the performance of longer scintillators. For instance, in a scintillator with a length of 200 cm, the typical length of a long strip for the KLM detector, the position with the poorest time resolution occurs at the midpoint, $Z_{\text{hit}} = 100$ cm, where the time resolution for single-end readout is approximately (140 ± 6) ps for GNKD_3. By leveraging time

information from both ends and averaging the data, we can achieve an improved time resolution of $140/\sqrt{2} \approx 98$ ps. This enhancement satisfies the time resolution requirement of the long plastic scintillators that can be used for the Belle II KLM upgrade [5].

5.4. Measurement of cosmic ray velocity

In our final endeavor, we developed an array using GNKD scintillators to measure the velocity of cosmic ray. We initially intended to employ plastic scintillators from batch GNKD_4 for cosmic ray velocity testing due to their superior time resolution demonstrated in previous experiments. As indicated in Table 1, the GNKD_4 scintillator demonstrates impressive time resolution performance, achieving 44 ps at the near end and 81 ps at the far end. With dual-end readout, the overall time resolution for the entire plastic scintillator improves to better than 47 ps, as illustrated in Fig. 8.

However, subsequent testing revealed inconsistent time resolution performance across individual scintillator bars within this batch, indicating that the production yield required improvement at the manufacturing level. Consequently, we ultimately selected 75 cm long scintillators from batch GNKD_1, which exhibited better stability, for the construction of the cosmic ray velocity testing platform. The signal readout was implemented using four serially SiPMs. Experimental results demonstrated that all scintillator bars achieved consistent time resolution of (120 ± 5) ps.

The prototype apparatus is illustrated in Fig. 9(a). Waveform acquisition is carried out using the CAEN digitizer DT5742. Initially, the four signals from the brief scintillation events are recorded simultaneously, and the logic signals are routed into TR0 of the DT5742 to serve as the system's trigger. The average time recorded at both ends of the scintillator corresponds to a particle's traversal duration.

Due to variations in timing across each electronic readout channel, the calibration of the test system's timing is performed using a pulsed laser. Emission from the laser at the midpoint of the scintillator reveals

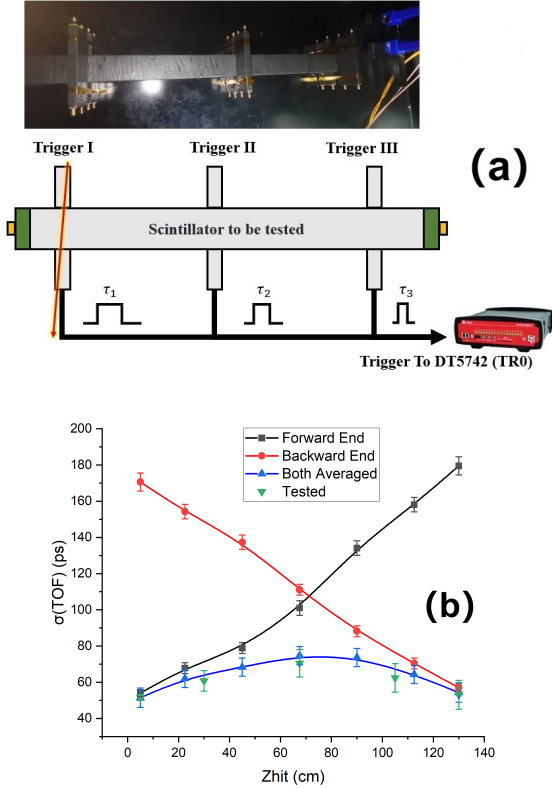


Figure 7: Plot(a) illustrates the schematic diagram of the multi-trigger test system. Plot(b) shows the time resolution as a function of the scintillator position. The red and black curves represent the single-ended time resolution. The blue curve corresponds to the calculation based on Eq. (2), while the green curve displays the time resolution results obtained from the weighted average of the times at both ends, with the trigger length reduced to 1 cm.

that the timing discrepancies for each channel predominantly arise from electronic variations. By establishing the timing of the initial long scintillator as a reference ($T_{SC1} = 0$ ps), we derive the temporal correlations for different positions and their corresponding impact times: $T_{SC2} \approx 27$ ps, $T_{SC3} \approx -70$ ps, $T_{SC4} \approx -56$ ps, $T_{SC5} \approx -111$ ps, and $T_{SC6} \approx 68$ ps. Using these baseline values, we can correct for electronics-induced discrepancies. After the time calibration, the measured velocity of muons is (29.958 ± 0.011) cm/ns, as shown in Fig. 9(b), corresponding to the energy of (2.8 ± 0.7) GeV for muons. The detection system achieves cosmic muon velocity measurements at 99.93 % the speed of light, demonstrating promising potential for high-time-resolution applications. Considering the energy loss of muons in the laboratory environment, this measurement aligns with the observed average muon energy range of 3–4 GeV[30].

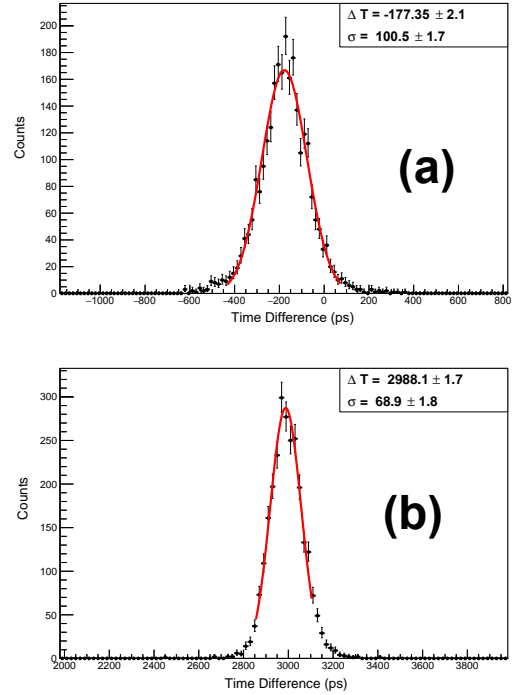


Figure 8: Time resolution test at the central position of the GNKD.4 scintillator using a dual-end readout scheme. (a) Gaussian fit of the time spectrum distribution from the trigger system, resulting in a time resolution of 50 ps. (b) Gaussian fit of the time spectrum distribution between T_0 and the dual-end readout scintillator, yielding a time resolution of 69 ps. After accounting for the contribution of the trigger system's time jitter, the scintillator's time resolution is determined to be 47 ps.

6. Conclusion

Inspired by the original design of Belle II, our approach integrates a solid-state scintillator with an extensive SiPM array and advanced readout electronics, significantly enhancing the detector's time resolution. Experimental investigations demonstrated that employing a series-parallel hybrid connection of SiPM arrays effectively reduces signal rise times, thereby improving overall time resolution. The time resolution of the scintillators is closely linked to the number of photons collected by the SiPMs. By increasing both the light yield and the light attenuation length, the dual-end readout of the GNKD.3 and GNKD.4 batches achieved impressive time resolutions of (70 ± 7) ps and (47 ± 2) ps, respectively, at the central position of the scintillator. These findings provide valuable reference data for future enhancements to the high time resolution capabilities of the Belle II KLM detector. Ultimately, we employed the scintillator to construct a prototype detector and mea-

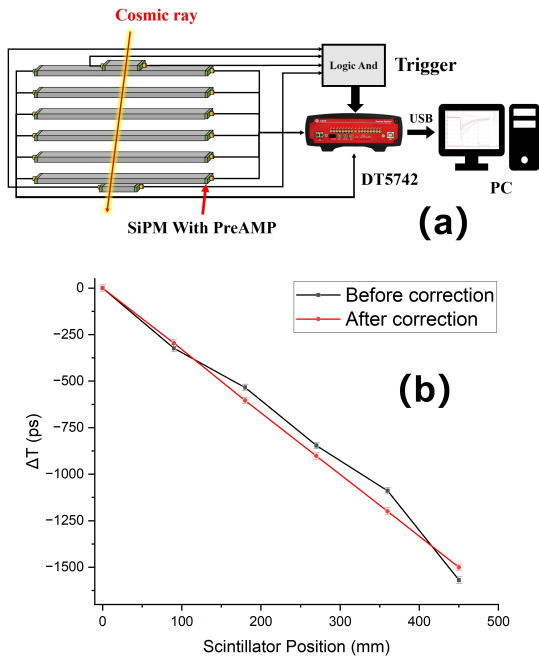


Figure 9: (a) Schematic of the prototype setup, which includes six long scintillators measuring $75 \text{ cm} \times 4 \text{ cm} \times 1.5 \text{ cm}$ and two short scintillators measuring $10 \text{ cm} \times 4 \text{ cm} \times 1 \text{ cm}$. The distance between each pair of long scintillators is 75 mm. (b) Comparison of cosmic ray velocity test results before and after applying time calibration corrections.

sure cosmic ray velocities to be $(29.958 \pm 0.011) \text{ cm/ns}$, corresponding to the energy of $(2.8 \pm 0.7) \text{ GeV}/c$ for muons. Future improvements in the production yield of scintillators could enable higher-precision muon velocity measurements through enhanced time resolution, while simultaneously providing energy distribution characterization.

References

[1] A. Airapetian *et al.* [ATLAS], CERN-LHCC-99-15.
[2] G. L. Bayatian *et al.* [CMS], J. Phys. G **34** (2007) no.6, 995-1579
[3] B. Aubert *et al.* (BABAR Collaboration), Nucl. Instrum. Methods A **479** (2002) 1.
[4] A. Abashian *et al.* (Belle Collaboration), Nucl. Instrum. Methods A **479** (2002) 117.
[5] H. Aihara *et al.*, *The Belle II Detector Upgrades Framework Conceptual Design Report*, arXiv: 2406.19421v1.
[6] M. Ablikim *et al.* (BESIII Collaboration), Nucl. Instrum. Methods A **614** (2010) 345.
[7] E. Kou *et al.*, Prog. Theor. Exp. Phys. **2019** (2019) 123C01.
[8] I. Adachi *et al.*, Nucl. Instrum. Methods A **907** (2018) 46.
[9] W.J. Llope *et al.*, Nucl. Instrum. Methods A **241** (2005) 306.
[10] A. Alici *et al.*, Nucl. Instrum. Methods A **706** (2013) 29.
[11] P. Cao *et al.*, Nucl. Instrum. Methods A **953** (2020) 163053.

[12] H. Kichimi *et al.*, Nucl. Instrum. Methods A **453** (2000) 315.
[13] Y. K. Heng *et al.*, IEEE Nucl. Sci. Symp. Conf. Rec. (2007): 53-56.
[14] M. Böhm *et al.*, J. Instrum. **11** (2016) C05018.
[15] C. Chung, Instruments **6** (2022) 14.
[16] Kuraray, Ltd. (Japan), <https://www.kuraray.com/products/psf>[Accessed 12 JAN 2024]
[17] BelleII VR, <http://www1.phys.vt.edu/~piilonen/VR/>
[18] F. Forti (for Belle II Collaboration), *Snowmass Whitepaper: The Belle II Detector Upgrade Program*, arXiv:2203.11349v1.
[19] A. Kazunori *et al.*, Nucl. Instrum. Methods A **907** (2018) 188
[20] H. Y. Zhang *et al.*, J. Instrum. **19** (2024) P06020.
[21] BC418-420-422 Datasheet, <https://luxiumsolutions.com/sites/default/files/2021-09/BC418-420-422%20Data%20Sheet>.
[22] GNKD website, <http://www.gaonengkedi.com/>
[23] Hamamatsu MPPC website, <https://www.hamamatsu.com/eu/en/product/optical-sensors/mppc/mppc.mppc-array.html>
[24] NDL, <http://www.ndl-sipm.net/>
[25] T. Cervi *et al.*, Nucl. Instrum. Methods A **912** (2018) 209.
[26] LMH6629 Datasheet, <https://www.ti.com/product/LMH6629>
[27] X. Y. Wang *et al.*, Nucl. Sci. Tech. **34** (2023) 169
[28] DT5742 16+1 Channel 12 bit 5 GS/s Switched Capacitor Digitizer, <https://www.caen.it/products/dt5742/>
[29] S. L. Li *et al.*, Chin. Phys. C **37** (2013) 016003.
[30] R. Bellotti *et al.*, Phys. Rev. D **35** (1996) 53.